A mixed dynamic optimization with μ-synthesis (D-K iterations) via optimal gain for varying dynamics of decoupled twin-rotor MIMO system based on the method of inequality (MOI). ⋆

Nadir Abbas * **Xiaodong Liu (c)** **

* *Department of Electronic Information and Electrical Engineering, Dalian University of Technology, Dalian, Liaoning, China (e-mail: nadir10@mail.dlut.edu.cn, nadirabbas063@gmail.com)*
** *Department of Electronic Information and Electrical Engineering, Dalian University of Technology, Dalian, Liaoning, China (e-mail: xdliuros@dlut.edu.cn)*

Abstract: The complex structured systems always demand efficient optimization to tackle all problems (constraints, parametric perturbation, multiobjective due to conflict of design), which must be achieved simultaneously. This paper provides the experimental validation of dynamic robust mixed optimization based on optimal gain for the varying constraints of a decoupled Twin Rotor MIMO System (TRMS). As mathematical models have unknown and unmatched nonlinear disturbances with un-modeled states during modeling, they need to be controlled to get the required response. Therefore, the design of a suitable controller for robust control of TRMS is a challenging task. The controller design process is divided into two phases to overcome this challenge. The first phase adopts the Nonlinear Dynamic Inversion (NDI) based decoupled linearization process to obtain the Vertical Plane System (VPS) and Horizontal Plane System (HPS). To reduce the disturbance, the diagonal matrix and decoupling methods are applied simultaneously. In the second phase, it covers the suitable choice of weighting functions (optimal gain) which uses the efficient order (reduced order) of the controller to provide a satisfactory optimal response. The weighting functions are applied as the design parameters. In this process, the weights are selected in such a way as to get the high gain for the low frequency and vice versa. The high gain actually depended on the choice of weighting functions which are chosen by considering the open-loop response of the weighted plant. In contrast, D-K iterations are performed to achieve the required output. The combined flexible approach with the μ-synthesis control as a mixed optimization makes it a mature algorithm to guarantee robust stability and robust performance at extreme disturbance. The experimental validation of this control strategy verifies the worth of the methodology due to the optimal selection of the values of tuning parameters. For practical implementation and validation of μ-synthesis, a Simulink/MATLAB coder is used.

Keywords: Perturbed MIMO system, robust stability performance, dynamic mixed optimization, optimal gain, D-K iterations.

1. INTRODUCTION

Applications for air vehicles caught interest due to their increasing control applications and flight control complexities. The modern control researchers are working on getting success in all such systems, which have some unknown non-linearities and un-modeled states of the TRMS Marconi and Naldi (2008); Lara et al. (2010). TRMS is a type of Unmanned Air Vehicle (UAV). Their ability to tilt their angle of flight, hovering, take-off, and landing in irregular locations provide special interest to researchers. A prototype of TRMS resembles a helicopter which can be served as an effective tool for experiments in a real-time environment Tastemirov et al. (2013). Highly coupled, a higher degree of nonlinear dynamics, uncertainties, and gyroscopic torque needs to be tackled by an effective, robust controller. The control theory researchers are attracted towards problems due to its ongoing expanding applications. Linear, nonlinear and intelligent control strategies are discussed as literature to understand the behavior of the TRMS as well as considered perturbations (noise, parametric) effect. Proportional Integral Derivative (PID) and Linear Quadratic Regulator (LQR) with out-

⋆ This research work is funded by the National Key R and D Program of China under Grant No. 2018YFB1702200 and National Natural Science Foundation (Grant No. 62076049). The content of this [report/study/article/publication] does not reflect the official opinion of the National Natural Science Foundation.

put feedback control are linear strategies implemented in Juang et al. (2008); Wen and Li (2011). The backstepping control strategy was also implemented to understand the behavior of the prototype in the presence of parametric uncertainties Haruna et al. (2017). Model Predictive Control (MPC) design also for TRMS presented with considering the matched, mismatched perturbations as disturbance Raghavan and Thomas (2017). Sliding Mode Control (SMC), Integral SMC, and second-order SMC are implemented Saroj et al. (2013); Young et al. (1999); Castanos and Fridman (2006). Chattering phenomena is the major disadvantage of the controller which may cause serious damage to the system. Adaptive second-order SMC is also discussed Liu and Juang (2009). TRMS verifies how important is to tackle this problem for a smooth output response Yu and Liu (2005). The experimental validation is also represented by a decentralized SMC strategy Faris et al. (2017). Intelligent control like the PID-based fuzzy sliding mode control is considered an excellent controller for such systems having some external disturbances mentioned in Huang et al. (2013). The neural networks control in Pratap and Purwar (2010) and RGDI-based robust controller in Abbas et al. (2022), make sure the convergence of highly nonlinear system towards equilibrium. Adaptive control with the combination of intelligent and nonlinear control is also revised to understand the pattern of the controller as well as the system behavior. Adaptive neural networks backstepping control in Liu et al. (2020) elaborated and adaptive fuzzy backstepping control discussed in Liu et al. (2017). Adaptive type-2 fuzzy backstepping control for the fractional-order nonlinear system is also studied in Jafari et al. (2019), to understand the worth of upcoming hot research in control. Such systems are focused due to their extending applications in a narrow environment for civil security and military operations Bucolo et al. (2020); Geranmehr et al. (2019). The controller design under some stability analysis discussed with coupling effect of a highly nonlinear system. Nonlinear Dynamic Inversion (NDI) is a feedback linearization tool for TRMS used to reduce the complexity of a mathematical model of TRMS Rahideh et al. (2012). Nonlinearities are canceled at any stability point by feedback linearization. The drawback of this method is that there may ignore some important nonlinearities, singularity, and square matrix inversion. Large systems always required efficient modeling, as well as numerical singularity avoidance in Bajodah et al. (2018); Ansari et al. (2016). Dynamic inversion before controller implementation provides a suitable environment to design the controller Ansari and Bajodah (2015); Ben-Israel and Greville (2003). The coupled nonlinear system is decoupled to have simplified sub-systems named Vertical Plane System (VPS) and Horizontal Plane System (HPS). Matched and mismatched uncertainties (perturbations) are also considered un-known disturbances. The significant coupling effect must be focused on to manage the stability complexities of the system. The un-modeled states and parametric perturbations with coupling effect are tasks for any efficient controller to regulate the output of all the states. The complex structured system always demands efficient optimization to tackle all problems (constraints, parametric perturbation, multiobjective due to conflict of design), which must be achieved simultaneously Whidborne et al. (1994); Mihaly et al. (2021). The contribution outline of the paper is enlisted as:

- The weighting functions (tuning parameters) are used as a design parameter. It will combine with μ-synthesis as a mixed optimization, to provide the combined benefits of optimization via the Method of Inequality (MOI).
- The diagonal matrix and decoupler are applied simultaneously (never implemented simultaneously) to reduce torque disturbance near to zero. As a reward, efficient tracking control is obtained.
- The flexible approach in term of design parameters make it a mature algorithm to guarantee robust stability and robust performance under extreme perturbations (external and internal disturbance).
- Real-time implementation under worse conditions (noise and parametric variation provided to both rotors simultaneously with disturbance torque) validates the worth of robust optimization, which shows better response as compared to present research.
- Some important suggestions for control engineers are provided on the basis of experimental validation, to understand the nature of control design as well as system behavior.

The remaining of this paper has the following sections as the mathematical modeling provided in section 2. The NDI process for constrained dynamics of the TRMS and the decoupling process is discussed in section 3. Section 4 provides unstructured modeling with block diagram representation. Section 5 elaborates on the mixed optimization design procedure to validate the robust optimization. The controller design preliminaries with simulation response discussion elaborated in section 6. Real-time setup description outline is explained in section 7 and the conclusion is based on the validated results with some suggestions for the control engineers presented in the last section of the article which is 8.

2. TWIN ROTOR MIMO SYSTEM (TRMS)

Twin Rotor MIMO System (TRMS) is a prototype whose structure is almost near to a helicopter with a limited degree of freedom. Modifications of such systems are required due to their wide applications in real life. The TRMS has two significant parts, the main rotor (vertical plane) and the tail rotor (horizontal plane). The main rotor with a higher diameter controls the movement of the beam on a vertical axis called pitch angle, while the tail rotor with a lower diameter covers the movement of the beam on a horizontal axis called yaw angle. The speed of the rotors manages the equilibrium of the system. Each rotor of the TRMS connected with a separate DC supply motor, as shown in figure 1. The rotational torque in the rotors of the TRMS produces cross-coupling torque to disturb the stability. This coupling effect is considered as the disturbance which is resolved by the decoupling process. The decoupling method is based on fixing one weight (motion) of both rotors, and the system is converted into two separate planes VPS and HPS. Before understanding mathematical modeling, we have to understand all varying parameters and required outputs of the TRMS. The TRMS is a lab apparatus that provides the under-

Fig. 1. Twin-Rotor Aerodynamic System.

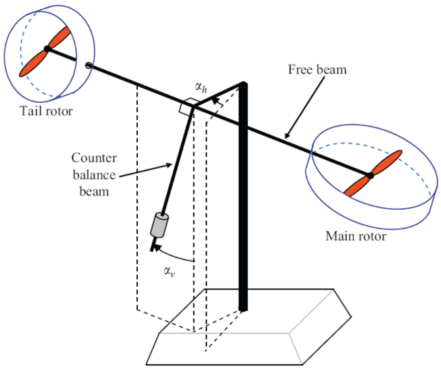

Fig. 2. Schematic Diagram of Twin-Rotor Aerodynamic System.

standing of the flight control of a helicopter Tastemirov et al. (2013). The considered system has two rotors as shown in figure 2 and their design is most important because different forces are affecting the movement of the propellers. These forces are gravitational force, propulsive force, centrifugal force, frictional force, and disturbance torque. To overcome the effects of these forces we provide control input voltage through motors. Understanding the mathematical assumptions, which are taken to understand and simplify the mathematical model. The rotor's dimensions are explained in figure 3 with their thrust directions: All nonlinear squared terms in the mathematical equations

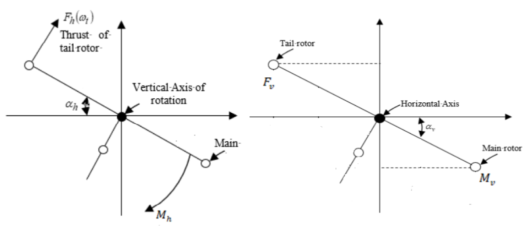

Fig. 3. Rotors dimensions with torque .

are linearized by the linearization process called NDI. The system movements are fixed along the horizontal plane and the azimuthal plane which are derived from the model Young et al. (1999). The rotational movement of the beam can be described as:

$$J_v \frac{d^2\alpha_v}{dt^2} = M_v \tag{1}$$

where M_v is considered as the whole momentum of the applied forces along the vertical plane, J_v shows the inertial momentum along the vertical plane axis. The parameter α_v is required one output to control, called pitch angle (vertical axis). All the forces of the momentum can be summarized by the following representation of the momentum as:

$$M_v = M_{v_1} + M_{v_2} + M_{v_3} + M_{v_4} + M_{v_5} + M_{v_d} \tag{2}$$

The gravitational torque through the gravitational force is given as:

$$M_{v1} = -k_1 cos\,(a_v) - k_2 sin\,(a_v) \tag{3}$$

where k_1 and k_2 show the constants which hold the mass mounted on the beam. The main propeller generates a momentum force which can be expressed through an equation as:

$$M_{v_2} = l_m F_v\,(w_v) \tag{4}$$

while l_m represents the length of the beam,w_v shows the rotational velocity of the main propeller, and $F_v(w_v)$ shows the angular force of the main rotor. The moment force along the vertical plane is represented by the mathematical equation given below:

$$M_{(v_3)} = -k_3 \Omega_h^2 sin(a_v) cos(a_v), \tag{5}$$

here, $\Omega_h = {}^{d\alpha_h}/_{d_t}$ is the beam velocity along the vertical plane of the MIMO system, α_h considered as the yaw angle (rotation of the beam along azimuth plane), and k_3 known as the constant coefficient. The frictional momentum depends upon the rotation of the beam with angular velocity in the horizontal plane:

$$M_{(v_4)} = -k_{f_v} \Omega_v, \tag{6}$$

here $\Omega_v = {}^{d\alpha_v}/_{d_t}$ represents the angular velocity along the horizontal plane, while k_{fv} shows the constant quantity. The momentum produced between the rotors due to applied input voltage (force) along the horizontal axis:

$$M_{(v_5)} = -k_{h_v} u_h, \tag{7}$$

where u_h is the horizontal axis control input and k_{hv} considered as the constant. The torque, generate disturbance called the disturbance torque M_{v_d} along the vertical axis. The propeller force (propulsive force) along the vertical axis (vertical plane) $F_v(w_v)$, produce the rotational velocity on the main rotor. The calculated velocity along the main rotor is given as:

$$\widetilde{F_v} = -7.13 \times 10^{-19} w_{v^5} - 3.79 \times 10^{-16} w_{v^4} + 2.41 \times 10^{-11} w_v^3 \\ +1.87 \times 10^{-8} w_v^2 + 2.89 \times 10^{-5} w_v - 0.0124$$

The summation of all the forces (torques) along the horizontal axis can be calculated on a vertical axis. The total torque produced by the tail rotor along the horizontal axis produces a force with a different spectrum (intensity of force). The torque (rotational effect of force) along a horizontal axis can be calculated by a mathematical expression given below:

$$J_h (d^2 a_h)/(dt^2) = M_h \tag{8}$$

where M_h is the total momentum (force) along horizontal axis, J_h is total inertial force along vertical plane, $J_h = k_4 cos2\,(\alpha v) + k_5$, the coefficients k_4 , k_5 are masses based constants of the beam. The total forces (momentum) along the horizontal axis are represented by a mathematical expression:

$$M_h = M_{h_1} + M_{h_2} + M_{h_3} + M_{h_d}, \tag{9}$$

All individual terms can be expressed as the propulsive momentum (force) along the tail rotor:

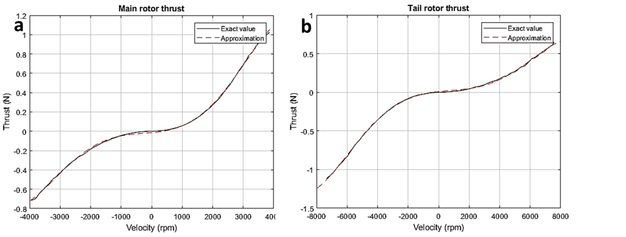

Fig. 4. 4(a) Main rotor thrust and 4(b) Tail rotor thrust.

$$M_{h_1} = l_t F_h\left(w_h\right) cos\left(a_v\right) \tag{10}$$

where l_t is beam length and w_h is the rotational velocity, $F_h(w_h)$ is the propulsive momentum (force) of the rotor with angular velocity. The frictional momentum based on the rotational velocity of the beam is described as,

$$M_{h_2} = -k_{f_h}\Omega_h \tag{11}$$

where k_{f_h} is a constant. The cross-sectional momentum due to control input action along the horizontal axis:

$$M_{h_3} = k_{v-h} cos\left(\alpha_v\right) u_v \tag{12}$$

where u_v is control input along the vertical axis, while k_{v_h} is a coefficient constant. The torque along the horizontal plane is represented as M_{h_d}, called the disturbance torque due to the tail rotor. The propeller force (propulsive force) along the horizontal axis (azimuthal plane) $F_v w_v$, produces the rotational velocity on the rotor. The calculated velocity along the tail rotor is given as:

$$\begin{aligned}\widetilde{F_h} = -2.56\times10^{-20}w_h^5 - 4.10\times10^{-17}w_h^4 + 3.17\times10^{-12}w_h^3\\ +7.34\times10^{-9}w_h^2 + 2.13\times10^{-5}w_h - 9.14,\end{aligned}$$

The equation of the main propeller (rotor) along the vertical plane can be described as:

$$I_v(dw_v)/dt = u_v - H_v^{-1}(w_v), \tag{13}$$

here I_v is the inertial momentum of the main rotor (along the vertical axis) and $w_v = H_v u_h$ shows the velocity (speed) of the main rotor known as the static velocity. The main rotor thrust is represented in figure 4a and the velocity simulation results based on the experimental validation shown in figure 4b. The 7th-order equation for the vertical plane velocity of the main rotor is given below:

$$\widetilde{w_v} = -6.17\times10^3u_v^7 - 1.30\times10^2u_v^6 + 1.37\times10^4u_v^5 + 1.50\times 10^2u_v^4 - 1.10\times10^4u_v^3 - 3.76\times10^1u_v^2 + 7.33\times10^3u_v - 5.36.$$

The tail rotor motion (speed) along the horizontal plane can be represented by a mathematical equation as:

$$I_h(dw_h)/dt = u_h - H_h^{-1}(w_h), \tag{14}$$

here I_h is the inertial momentum of the tail rotor (along the horizontal axis) and $w_h = H_h u_h$ shows the velocity (speed) of the main rotor known as the static velocity. The tail rotor thrust and the velocity simulation results are based on experimental validation. The 5th-order equation of the rotational velocity is given below:

$$\begin{aligned}\widetilde{w_h} = -6.17\times10^3u_h^5 - 1.30\times10^2u_h^4 + 1.37\times10^4u_h^3\\ +1.50\times10^2u_h^2 - 1.10\times10^4u_h - 37.6.\end{aligned}$$

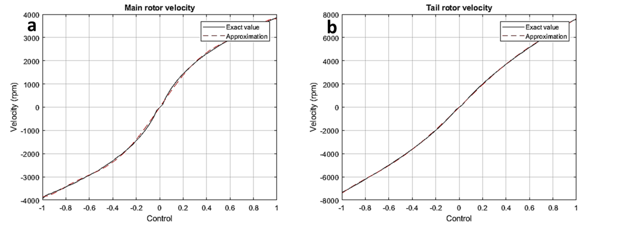

Fig. 5. 5(a) Main rotor velocity and 5(b) Tail rotor velocity.

By rearranging both equations (13) and (14) together:

$$\frac{d\alpha_v}{dt} = \Omega_v \tag{15}$$

$$\frac{d\alpha_h}{dt} = \Omega_h \tag{16}$$

The state space model of the TRMS (6th order nonlinear system) is represented in the mathematical modeling with the control input voltages u_h (horizontal plane or yaw angle) and u_v (vertical plane or pitch angle). The output angles are yaw (azimuth) angle α_h and pitch (vertical) angle α_v. To understand the full dynamic response of the system, it must be categorized as a multivariable system with highly nonlinear behavior. The TRMS model has two channels which can never be considered independent channels. This cross-coupled property is known as the coupling effect. The coupling effect must be countered by a decoupling procedure and converted it into the independent two-channel system. The system coefficient values of the model are enlisted in table 1.

Table 1. Parameters of TRMS.Cheng et al. (2018)

Symbol	Description	Unit
I_v	1/6100	kgm^2
I_h	1/37000	kgm^2
J_v	3.00581×10^{-2}	kgm^2
k_1	5.00576×10^{-2}	Nm
k_2	9.0036×10^{-2}	Nm
k_3	2.12485×10^{-2}	Nms^2/rad^2
k_4	$2.3790412485\times10^{-2}$	kgm^2
k_5	3.00962×10^{-3}	kgm^2
k_{f_h}	5.88996×10^{-3}	$Nm-s/rad$
kf_v	1.27095×10^{-2}	$Nm-s/rad$
k_{h_v}	4.17495×10^{-3}	Nm
k_{v_h}	-1.7820×10^{-2}	Nm
l_m	0.202	m
l_t	0.216	m

3. NONLINEAR DYNAMIC INVERSION (NDI) AND DECOUPLING

Feedback linearization control is also known as NDI control which establishes a supporting platform for linear control. The basic idea to embed this strategy is the cancellation of nonlinear terms as well as having a simplified mathematical model. Different variables about the angular position are described in a given form:

$\alpha_v = \alpha_{v,nom} + \delta\alpha_v,\quad w_v = w_{v,nom} + \delta w_v,\quad \Omega_v = \Omega_{v,nom} + \delta\Omega_v$

$\alpha_h = \alpha_{h,nom} + \delta\alpha_h,\quad w_h = w_{h,nom} + \delta w_h,\quad \Omega_h = \Omega_{h,nom} + \delta\Omega_h$

where $\alpha_{v,nom}, w_{v,nom}, \Omega_{v,nom}, \alpha_{h,nom}, w_{h,nom}, \Omega_{h,nom}$ represents the corresponding values and $\delta\alpha_v, \delta w_v, \delta_{\Omega v}, \delta\alpha_h, \delta w_h$, $\delta_{\Omega h}$ shows deviations from nominal values. The motor voltages are shown as $u_v = u_{v,nom} + \delta u_v, u_h = u_{h,nom} + \delta u_h$, All the output states are supposed to be converged at the origin, $\Omega_{h,nom} = 0, \Omega_{v,nom} = 0$. After some basic mathematical operations and assumptions, given in Cheng et al. (2018), linearized system equations are obtained here:

$$I_v \frac{d\delta w_v}{dt} = \delta u_v - \left({}^1\!/_{k_{H_v}} \right) \delta w_v \tag{17}$$

$$I_h \frac{d\delta w_h}{dt} = \delta u_h - \left({}^1\!/_{k_{H_h}} \right) \delta w_h \tag{18}$$

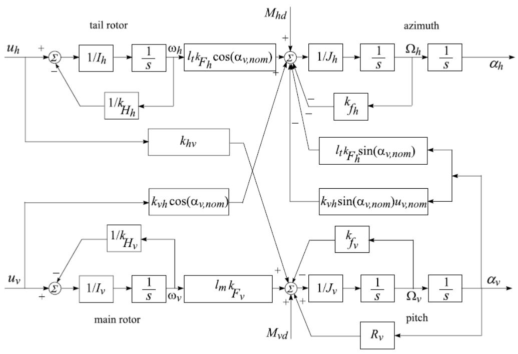

Fig. 6. Open loop block diagram of TRMS .

The block diagram of the TRMS system with the coupling effect is represented in figure 6. The cross-coupling effect with all other unwanted perturbations makes the TRMS behavior very complex. The horizontal plane angle can be fixed by posing the value of $u_h = 0$. Decoupling makes the system into subsystems such as VPS and HPS Loutfi et al. (2019). The transfer function of both subsystems is given below:

$$G_v(s) = \frac{111.2}{0.390s^3 + 0.3835s^2 + 1.454s + 1} \tag{19}$$

$$G_h(s) = \frac{111.2}{5.64s^2 + 3.97s + 1} \tag{20}$$

Subsystems are obtained by putting second control input equal to zero. The NDI can be affected by the singularity during the inversion process. The rank of the system matrix will be changed which generates a discontinuous behavior, which tends to go elements in the matrix unbounded. Such kind of drawbacks can be covered by augmentation of scaling factor in Ansari and Bajodah (2016), elaborated as:

$$\dot{v}(t) = -v(t) + \frac{\gamma}{e_z(t)^2},\ v(0) > 0 \tag{21}$$

where γ is constant while $e_z(t)$ represents the tracking of pitch angle and yaw angle. A negative sign represents the convergence towards origin and asymptotic stability confined in equation 24 with tracking control of the angles in the above expression.

4. UNSTRUCTURED MODELING

The varying structure type systems always have some unknown states and mathematical complexities during modeling. The description of uncertain parameters is represented in mathematical expressions and notations. We suppose that J_h is inertial momentum along the horizontal axis and k_{F_h}, k_{F_v} are coefficients of the generated thrust of rotors. Rotors have some velocity gains k_{H_h}, k_{H_v}. The coefficients, k_{f_h}, k_{f_v} and k_{v_h}, k_{h_v} are frictional momentum as well as cross momentum coefficients respectively. R_V is returned torque (coupling effect) between rotors. All these 10 modeled parameters have a dependency on our main two outputs named pitch angle and yaw angle.

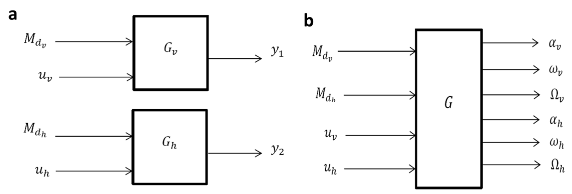

Fig. 7. 7(a) Block diagram of decoupled TRMS input/output and 7(b) Block diagram of coupled TRMS input/output .

In addition, we suppose that the inertial momentum J_h, with coefficients $k_{F_h}, k_{F_v}, k_{H_h}, k_{H_v}$, have the error estimation up to 10%. The remaining coefficients have an error estimation of up to 5%. The mathematical expressions of the TRMS represent the system behavior as the controlled plant:

$$G = \begin{bmatrix} G_v \\ G_h \end{bmatrix} \tag{22}$$

where,

$$y = G \begin{bmatrix} M_d \\ u \end{bmatrix}, y = \begin{bmatrix} \alpha_h \\ \alpha_v \end{bmatrix}, u = \begin{bmatrix} u_h \\ u_v \end{bmatrix}, M_d = \begin{bmatrix} M_{d_h} \\ M_{d_v} \end{bmatrix} \tag{23}$$

The system schematic model of the TRMS with their input-output connections are represented in the figure 7a and figure 7b. Now, the basic mathematical description of the uncertain model is discussed below. Let us introduce the representation, $G = [\, G_d \ G_u \,]\, while$, $G_d = [\, G_{d_h} \ G_{d_v} \,]$ $\quad G_u = [\, G_{u_h} \ G_{u_v} \,]$

such that

$$y = G_d M_d + G_u u \tag{24}$$

According to the above expression, G_d represents the disturbance of the plant as a matrix and G_u shows the transfer matrix of the control signal. The singular value of the uncertain plant (nonlinear plant) is represented in the figure 8, which is the frequency response of the system. The un-certain plant has some basic requirements in the presence of perturbations (internal and external disturbance):

$$u = [\, K_r \ K_y \,] [\, r \ -y_c \,]^T = K_r r - K_y y_c \tag{25}$$

where K_y represents the feedback matrix function and K_r is the transfer function matrix of the pre-filter.

5. MIXED OPTIMIZATION WITH ROBUST PERFORMANCE VALIDATION

The optimal gain actually depended on the choice of weighting functions which are chosen by considering the open-loop response of the weighted plant, so effectively the weights W_p and W_u are the design parameters. This

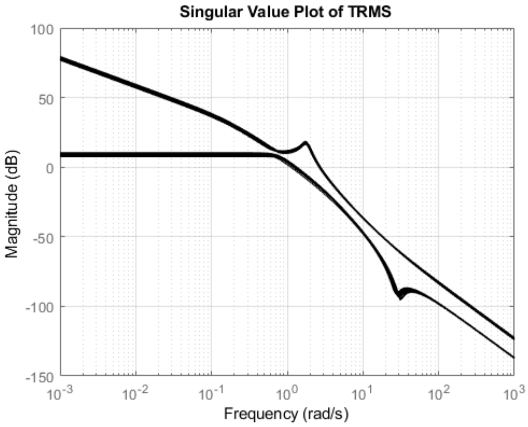

Fig. 8. Singular value of TRMS

means that the design problem can be formulated as in the method of inequalities, with the parameters of the weighting functions used as the design parameters to satisfy the set of closed-loop performance inequalities. Such an approach to the MOI overcomes its limitations of the MOI. The designer does not have to choose the order of the controller but instead chooses the order of the weighting functions. With low-order weighting functions, high-order controllers can be synthesized which often leads to significantly better performance or robustness than if simple low-order controllers were used. The design problem is now stated as follows. Design Procedure 1. Define the plant G_v, G_h and define the function. 2. Define the values of e_y and e_z. 3. Define the form and order of the weighting functions W_p and W_u. Bounds should be placed to ensure that W_p and W_u are stable and minimum phase to prevent undesirable pole/zero cancellations. The order of the weighting functions, and hence the value should be small initially. 4. Define initial values of W_p based on the open-loop frequency response of the plant. 5. Implement the MBP, or other appropriate algorithms to find a (W_p, W_u) that satisfies inequalities. If a solution is found, the design is satisfactory; otherwise, either increase the order of the weighting functions, or relax one or more of the desired bounds, or try again. 6. With satisfactory weighting functions W_p and W_u, a satisfactory feedback controller is obtained. The term optimal gain means the high gain actually depended on the choice of weighting functions which are chosen by considering the open-loop response of the weighted plant, so effectively the weights W_p and W_u are the design parameters. This means that the design problem can be formulated as in the method of inequalities, with the parameters of the weighting functions used as the design parameters to satisfy the set of closed-loop performance inequalities. Different variables like "r", "d", and "n" represent the reference input, input disturbance, and noise respectively. Output angles such as yaw angle α_h and pitch angle α_v are required to control (measure) under all kinds of perturbations (noise, parametric, coupling effect). Output tracking control signals e_y and e_u are error tracking signals. The output feedback vector $y_c = y + W_{nn}$, is the vector-matrix having measured noise n and W_n filter for the noise shaping. Following weighted functions of the system required error tracking output (e_y *and* e_u), equation must satisfy the condition:

$$\begin{bmatrix} e_y \\ e_u \end{bmatrix} =$$

$$\begin{bmatrix} W_p\left(S_o G_u K_r - M\right) & W_p S_o G_d & -W_p S_o G_u K_y W_n \\ W_u S_i K_r & -W_u S_i K_y G_d & -W_u S_i K_y W_n \end{bmatrix} \begin{bmatrix} r \\ d \\ n \end{bmatrix}$$

while $S_i = (I + K_y G_u) - 1$ and $S_o = (I + G_u K_y) - 1$ shows input, output sensitivity matrix function respectively.The following conditions are achieved,

- Robust Performance < 1, for structured uncertainty
- Robust Stability < 1, for structured uncertainty
- Nominal Performance < 1
- Nominal Stability. G is internally stable

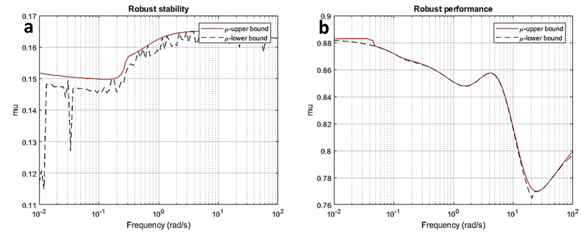

Fig. 9. 9(a) Robust stability 9(b) Robust Performance.

Table 2. Weighted Functions.

Functions	Description
$W_p(S_o G_u K_r - M)$	Weighting difference
$W_p S_o G_d$	Weighted sensitivity to disturbance
$W_p S_o G_u K_y W_n$	Weighted sensitivity to noise
$W_u S_i K_r$	Weighted control action due to reference
$W_u S_i K_y G_d$	Weighted control action due to disturbance
$W_u S_i K_y W_n$	Weighted control action due to noise

The performance criterion requires the transfer function matrix from the exogenous input signals r, d and n to the output signals e_y and e_u to be small, for all the possible output of uncertain plant model G. The transfer function matrices W_p and W_u are used to reflect the relative importance of different frequency ranges for which the performance requirements should be fulfilled. The transfer function matrices which constitute the transfer function matrix between the inputs and outputs of the extended system are described in table 2. The controller design task is to regulate the required output:

$$K = [K_r \qquad K_y] \tag{26}$$

That must elaborate and satisfy the enlisted properties under perturbations Callier and Desoer (2012). Robust stability under perturbations must meet the required response by satisfying closed-loop nominal performance and robust response conditions as mentioned Jastrzebski et al. (2011); Morari and Zafiriou (1989). The condition for nominal performance:

$$\left\| \begin{bmatrix} W_p\left(S_{o,nom} G_{u,nom} K_r - M\right) & W_p S_{o,nom} G_{d,nom} & -W_p S_{o,nom} G_{u,nom} K_y W_n \\ W_u S_{i,nom} K_r & -W_u S_{i,nom} K_y G_{d,nom} & -W_u S_{i,nom} K_y W_n \end{bmatrix} \right\|_\infty < 1 \tag{27}$$

The condition for robust performance:

$$\left[\begin{array}{ccc} W_p\left(S_oG_uK_r - M\right) & W_pS_oG_d & -W_pS_oG_uK_yW_n \\ W_uS_iK_r & -W_uS_iK_yG_d & -W_uS_iK_yW_n \end{array}\right]_\infty < 1 \quad (28)$$

The above conditions must be satisfied for G.The closed-loop model (uncertain TRMS) shown in figure 9a, represents the controller stability response, performance requirement, and disturbance matrix of the noise function. While figure 9b represents the robust performance.

6. CONTROLLER DESIGN PRELIMINARIES

The basic controller design with its attributes is covered in this section. This section elaborates on the appropriate system's controller with all possible weighting functions. The structured and unstructured perturbations with nominal robust performance requirements are achieved by a robust optimization strategy. The controller design of a higher-order variable structure system is a very important and extremely complicated task. The stability of complex systems needs concentration towards system stability analysis as discussed Doyle (1982); Ng (1988). Quality of work and the increasing response of production, make it more popular. The mathematical model of any VSS-type system represents the dynamics. The MIMO systems like TRMS are higher-order systems with highly nonlinear behavior. A mixed optimization method based on MOI provides flexibility in term of controller design specifications. For example, the controller for the system may be required to have a rise time of less than one second, a settling time of fewer than five seconds, and an overshoot of less than 10 *percent*. In such cases, it is obviously more logical and convenient if the design problem is expressed explicitly in terms of such inequalities. The method of inequalities Zakian and Al-Naib (1973) is a computer-aided multiobjective design approach, where the desired performance is represented by such a set of algebraic inequalities and where the aim of the design is to simultaneously satisfy these inequalities.

The μ-synthesis is the robust control strategy that mitigates the perturbations to get the required results. The outline for the design of the strategy contains two steps, first one is to derive robust performance in the presence of structured and unstructured perturbations which would be transformed towards stabilization. The next step is about the design specifications of the iterative method Gu et al. (2005). $D-K$ iteration based μ-synthesis method as shown in the figure 10, based on weighting functions to ensure the credibility of control strategy Slavov et al. (2013); Doyle (1985). The controller design contains four major steps which are elaborated in figure 11. The robust control toolbox is used to verify the functions property "*dksyn*". The basic idea of $D - K$ iteration is to find an optimal controller (K) and an optimal scaling (D) in an iterative way, Their aspects are related (required) to reduce the cost value of the singular value function. The function, $P_d\left(z\right) = F_U\left(N_d, \delta\right)$, represents the transfer function of discrete open loop TRMS.

The block structure of the ΔP_d can be elaborated here by a mathematical equation given below:

$$\Delta P_d := \left\{\left[\begin{array}{cc} \Delta & 0 \\ 0 & \Delta_F \end{array}\right] : \Delta \in \mathcal{R}^{10\times10},\ \Delta_F \in C^{6\times4}\right\} \quad (29)$$

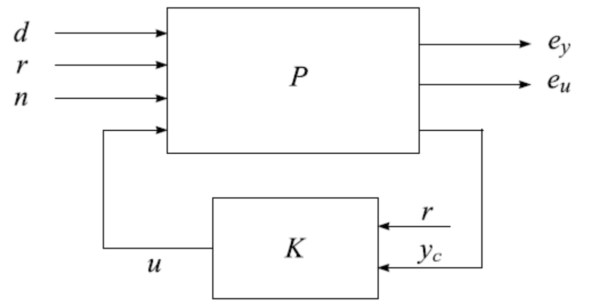

Fig. 10. Block diagram of controller

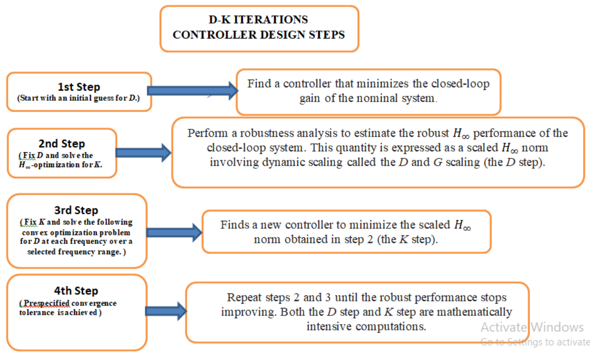

Fig. 11. Controller design flow chart.

The parametric uncertainties as a block, are being notified by ΔP_d and Δ in the mathematical expression. The fictitious perturbation block is Δ_F, containing robust performance for $\mu-$approach. The controller task is to get the discrete stabilizing controller to gain K_d, which must satisfy the condition:

$$\mu_{\Delta_{P_d}}\left[F_L\left(N_d, K_d\right)(j\omega)\right] < 1 \quad (30)$$

where $F_L(N_d, K_d)$ is the transfer matrix of the closed-loop dynamic system. The robust based performance of the system must have limited output which is less than one, i.e.

$$F_U\left[F_L\left(N_d, K_d\right), \Delta P_d\right]_\infty < 1 \quad (31)$$

The decoupled system can never be purely decoupled during real-time implementation. The ideal model is selected as a diagonal matrix to reduce the coupling effect of the system as,

$$M\left(s\right) = \left[\begin{array}{cc} \omega_{m1} & 0 \\ 0 & \omega_{m2} \end{array}\right] \quad (32)$$

$$\omega_{m1} = \frac{1}{1.2s^2 + 1.1s + 1} \quad (33)$$

$$\omega_{m2} = \frac{1}{1.8s^2 + 1.5s + 1} \quad (34)$$

The magnitude response of the azimuth angle magnitude response is faster than the pitch angle magnitude response. Several iterations are performed, several times to get the optimal response under all nonlinearities (parametric, modeling error, noise signal) of the system Cheng et al. (2018). The weighting functions are known as tuning parameters to get the best performance. The experimental evidence-based weighting (tuning parameters) functions are defined here:

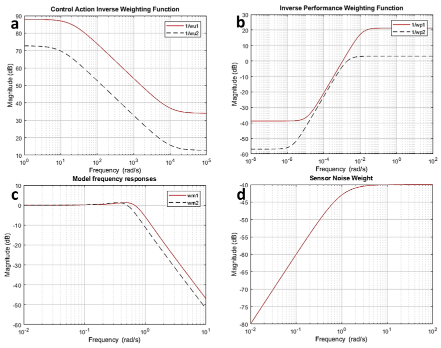

Fig. 12. 12(a) Inverse weighting function 12(b) Inverse performance 12(c) Model Frequency 12(d) Sensor noise

$$W_P(s) = \begin{bmatrix} 8.5 \times 10^{-2} \dfrac{80s+1}{80s+10^{-3}} & -0.03 \\ 0.02 & 7.0 \times 10^{-1} \dfrac{501s+1}{501s+10^{-3}} \end{bmatrix} \quad (35)$$

The weighting (tuning parameters) function for the input control signal is given below:

$$W_u(s) = \begin{bmatrix} 4.1 \times 10^{-5} \dfrac{0.05s+1}{10^{-4}s+1} & 0 \\ 0 & 2.306 \times 10^{-4} \dfrac{0.1s+1}{10^{-4}s+10^{-3}} \end{bmatrix} \quad (36)$$

The tuning parameters (weighting function) for both angles are chosen to limit the output variation within $[-0.8, 0.8], [-0.5, 1]$ for the azimuth angle and the pitch angle respectively.

The inverse performance functions, inverse control functions are represented in the figure 12a and figure 12b respectively. The weighting functions (tuning parameters) are selected on the basis of required constraints. The closed-loop system response on the basis of experimental evidence is very sensitive. The large number of experiments is required to get the best weighting function value. Precise tuning for the weighting function is the key point for the optimal robust response. The transfer function of the noise matrix is given below:

$$W_n(s) = \begin{bmatrix} \omega_n(s) & 0 \\ 0 & \omega_n(s) \end{bmatrix} \quad (37)$$

where the noise transfer function matrix $\omega_n = 10^{-2}\frac{s}{s+1}$ worked as high pass filter with the significant output more than 10 rad/s. The model frequency response and noise matrix signal response shown in figure 12c and figure 12d respectively. The D–K iterations are shown in table 3.

Table 3. D-K Iterations.

Iterations	Controller order	value of μ
1	16	232.315
2	16	4.942
3	20	1.336
4	22	0.986
5	24	0.969

Limited iterations are performed as mentioned in the above table, which reduces the cost value up to 0.968 with the 24th order of controller. The decoupled system response based on robust stability as well as robust performance is validated in figure 13a and figure 13b respectively. The system output can be disturbed by noises at frequency ranges from 5 rad/s to 10 rad/s. The decoupled TRMS output response shows that this effect is negligible due to the decoupler and diagonal matrix. The step input is provided to express the decoupled system response under perturbations (structured and unstructured).

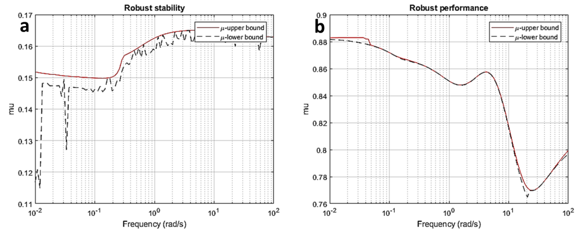

Fig. 13. 13(a) Robust Stability, 13(a) Robust performance

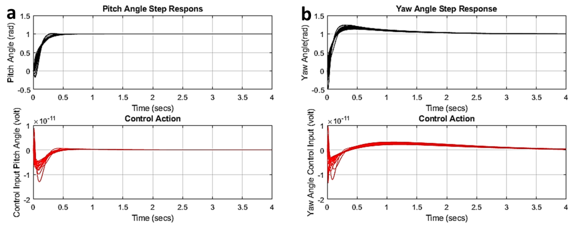

Fig. 14. 14(a) Pitch Angle With Control Action, 14(b) Yaw Angle With Control Action

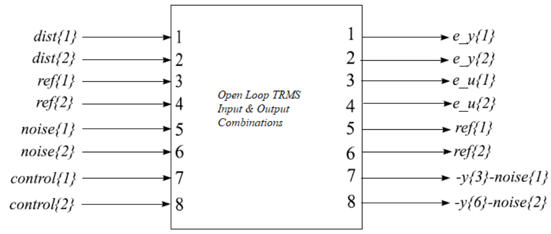

Fig. 15. System Internal Structure of Open Loop TRMS

Pitch angle as well as yaw angle with their control input response elaborated in figure 14a and figure 14b respectively. The structure of the open-loop system with all input-output (8/8) ports is represented in figure 15.

7. EXPERIMENTAL SETUP WITH SYSTEM INTERNAL STRUCTURE

In this section, we elaborate on the key concept of real-time implementation and system interconnections through system-integrated circuits. The internal structure of the system is also labeled with ports, to understand implementation more precisely to the reader. The open-loop system block diagram with their reference input points and required output ports is represented in figure 16.

The schematic diagram of the closed-loop system with important variables description elaborated in figure 17 and a number of input-output ports also provided to understand the internal structure easily. The block diagram of closed-loop system interconnections with a short description elab-

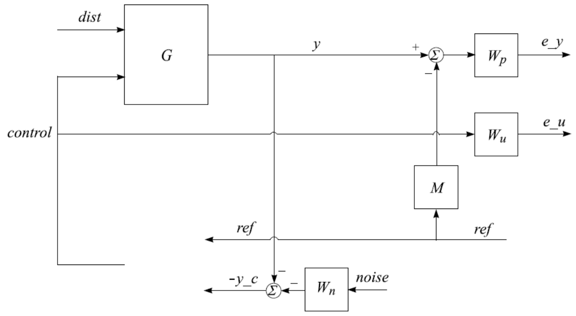

Fig. 16. Open Loop Block Diagram With Input/Output Scheme

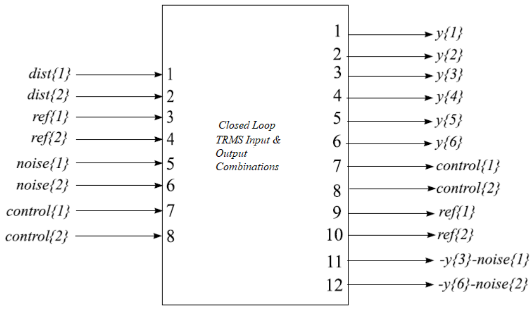

Fig. 17. System Internal Structure of Closed Loop TRMS

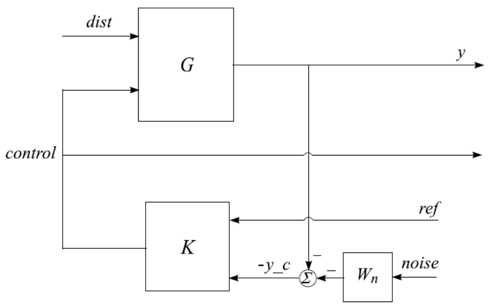

Fig. 18. Closed Loop Block Diagram With Input/Output Scheme

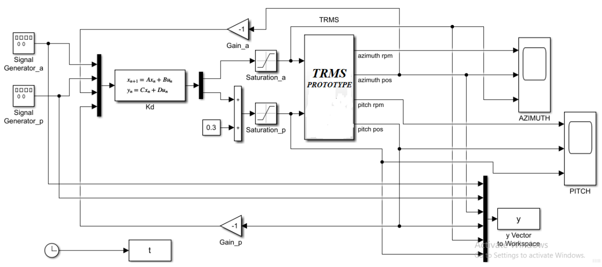

Fig. 19. Experimental Setup With Prototype.

orated in figure 17 and the direction of the arrow showing the signal flow of TRMS in figure 18.

The real-time implementation with the help of a robustly designed controller validates the controller worth under disturbances (noise signal, un-modeled states, parametric, coupling effect). Experimental setup connected with a personal computer is represented in figure 19, implemented for closed-loop systems via a built-in drive interface.

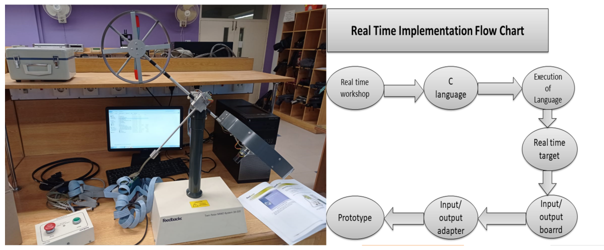

Fig. 20. Flow Chart TRMS Laboratory Setup Implementation.

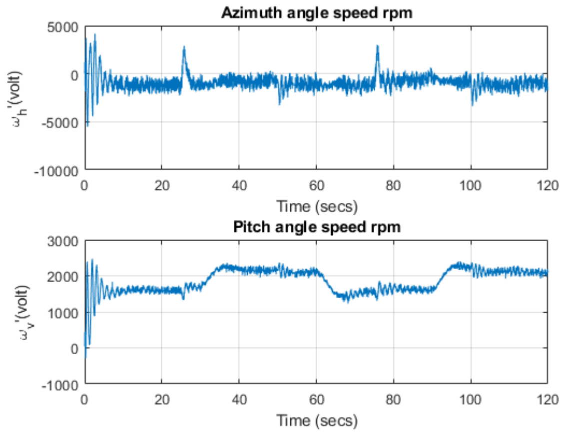

Fig. 21. Rotors Speed (rpm).

The experimental processing setup of TRMS with all required steps is mentioned in figure 20 to understand the laboratory hardware prototype implementation. The reference speed (velocity) variations provided to azimuthal angle (tail rotor) and pitch angle (main motor) with limited amplitude are represented in figure 21. The limited varying speed is provided to validate the system's robust response with the stability and credibility of the controller. The experimental output response of the pitch angle and yaw angle with their control action shows in figure 22 and figure 23 that validates the system's sharp response towards convergence within a limited variation range of voltage. Experimental results describe that linearized systems have the almost same response as compared to nonlinear system responses. A high level of noise (disturbance), causes a serious problem with the actuators and input control signal as an error. To get the actual actuator input the first-order filter based on the Butterworth filter was used.

8. CONCLUSION

The work reported in this paper is the outcome of several attempts to design a robust controller and robust performance for the coupled TRMS, which is a prototype model of a helicopter. This model is a higher-order system having a significant coupling effect between the main (pitch) rotor and tail (yaw) rotor. The design of a suitable controller for the robust control of the TRMS is a challenging task. Due to nonlinearities in the system, some assumptions have been made while deriving its mathematical model. The dynamic inversion process reduces the complexity behind the mathematical model assumptions and stability analysis (stability performance and robust performance) provides

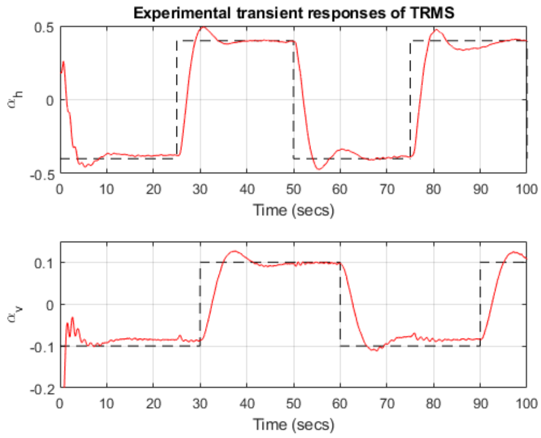

Fig. 22. Experimental Response of TRMS .

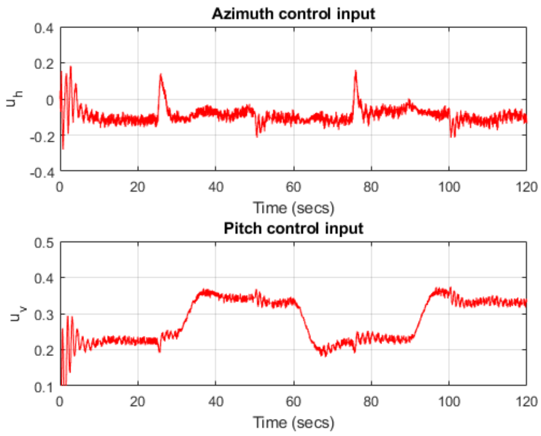

Fig. 23. Experimental Response of Control Action .

a satisfactory response to design a robust optimization. The weighting functions are used as design parameters, which have been selected for the robust control of varying constraints of the system so that high gains have been achieved for the low frequency and low gains achieved for the high frequency. The weights have been selected iteratively through the stability and robustness performance simulation results behavior. The system output can be disturbed by noises at frequency ranges from 5 rad/s to 10 rad/s. The decoupled TRMS output response shows that this effect is negligible due to the decoupler and diagonal matrix. Under such conditions, the system must be controlled with an efficient sharp response, which is the objective of this research work. The real-time implementation validates the worth of the control strategy by converging output response in the presence of perturbations (noise signal, un-modeled states, parametric, coupling effect). The research experience about the controller design (D-K iterations) and real-time implementation verifies that the decoupled TRMS has the following suggestions for control engineers.

- The modern control research for real-time implementation in this paper verifies that the controller must be of higher order ($n = 24$). The higher-order controllers have the best performance for the highly nonlinear coupled system.
- Noise signals with high amplitude cause serious contamination for input actuators and high range frequency.
- The disturbance torque of the tail rotor cannot be reduced to zero through the decoupling process in real-time performance.
- The controller report verifies the robust stability as well as the robust performance of modeled perturbations (uncertainty). The maximum tolerance ability against perturbations is more than 500%.
- There is no instability caused at the frequency 0.001 rad/s due to modeled perturbation.
- The system's robust margin against performance is 1.051. The robust performance margin is o.968 in terms of model perturbation exist with a size up to 103% at 22.3 rad/s.

ACKNOWLEDGEMENTS

This research work is funded by the National Key R and D Program of China under Grant No. 2018YFB1702200. The content of this [report/study/article/publication] does not reflect the official opinion of the National Natural Science Foundation.

REFERENCES

Abbas, N., Pan, X., Raheem, A., Shakoor, R., Arfeen, Z.A., Rashid, M., Umer, F., Safdar, N., and Liu, X. (2022). Real-time robust generalized dynamic inversion based optimization control for coupled twin rotor mimo system. *Scientific Reports*, 12(1), 1–17.

Ansari, U. and Bajodah, A.H. (2015). Generalized dynamic inversion scheme for satellite launch vehicle attitude control. *IFAC-PapersOnLine*, 48(9), 114–119.

Ansari, U. and Bajodah, A.H. (2016). Guidance and robust generalized inversion based attitude control of satellite launch vehicle. In *2016 4th International Conference on Control Engineering & Information Technology (CEIT)*, 1–6. IEEE.

Ansari, U., Bajodah, A.H., and Alam, S. (2016). Generalized dynamic inversion based attitude control of autonomous underwater vehicles. *IFAC-PapersOnLine*, 49(23), 582–589.

Bajodah, A.H., Mibar, H., and Ansari, U. (2018). Aircraft motion decoupling of roll and yaw dynamics using generalized dynamic inversion control. In *2018 26th Mediterranean Conference on Control and Automation (MED)*, 1–9. IEEE.

Ben-Israel, A. and Greville, T.N. (2003). *Generalized inverses: theory and applications*, volume 15. Springer Science & Business Media.

Bucolo, M., Buscarino, A., Fortuna, L., and Gagliano, S. (2020). Bifurcation scenarios for pilot induced oscillations. *Aerospace Science and Technology*, 106, 106194.

Callier, F.M. and Desoer, C.A. (2012). *Linear system theory*. Springer Science & Business Media.

Castanos, F. and Fridman, L. (2006). Analysis and design of integral sliding manifolds for systems with unmatched perturbations. *IEEE Transactions on Automatic Control*, 51(5), 853–858.

Cheng, Y., Chen, Z., Sun, M., and Sun, Q. (2018). Cascade active disturbance rejection control of a high-purity distillation column with measurement noise. *Industrial & Engineering Chemistry Research*, 57(13), 4623–4631.

Doyle, J. (1982). Analysis of feedback systems with structured uncertainties. In *IEE Proceedings D-Control Theory and Applications*, volume 129, 242–250. IET.

Doyle, J.C. (1985). Structured uncertainty in control system design. In *1985 24th IEEE Conference on Decision and Control*, 260–265. IEEE.

Faris, F., Moussaoui, A., Djamel, B., and Mohammed, T. (2017). Design and real-time implementation of a decentralized sliding mode controller for twin rotor multi-input multi-output system. *Proceedings of the Institution of Mechanical Engineers, Part I: Journal of Systems and Control Engineering*, 231(1), 3–13.

Geranmehr, B., Khanmirza, E., and Kazemi, S. (2019). Trajectory control of aggressive maneuver by agile autonomous helicopter. *Proceedings of the Institution of Mechanical Engineers, Part G: Journal of Aerospace Engineering*, 233(4), 1526–1536.

Gu, D.W., Petkov, P., and Konstantinov, M.M. (2005). *Robust control design with MATLAB®*. Springer Science & Business Media.

Haruna, A., Mohamed, Z., Efe, M.Ö., and Basri, M.A.M. (2017). Dual boundary conditional integral backstepping control of a twin rotor mimo system. *Journal of the Franklin Institute*, 354(15), 6831–6854.

Huang, Y., Wu, H., and Kuo, T. (2013). Pid-based fuzzy sliding mode control for twin rotor multi-input multi-output systems. In *IEEE 2013 Tencon-Spring*, 204–207. IEEE.

Jafari, A.A., Mohammadi, S.M.A., and Naseriyeh, M.H. (2019). Adaptive type-2 fuzzy backstepping control of uncertain fractional-order nonlinear systems with unknown dead-zone. *Applied Mathematical Modelling*, 69, 506–532.

Jastrzebski, R.P., Smirnov, A., Pyrhönen, O., and Piłat, A.K. (2011). Discussion on robust control applied to active magnetic bearing rotor system. *Challenges and Paradigms in Applied Robust Control*.

Juang, J.G., Huang, M.T., and Liu, W.K. (2008). Pid control using presearched genetic algorithms for a mimo system. *IEEE Transactions on Systems, Man, and Cybernetics, Part C (Applications and Reviews)*, 38(5), 716–727.

Lara, D., Romero, G., Sanchez, A., Lozano, R., and Guerrero, A. (2010). Robustness margin for attitude control of a four rotor mini-rotorcraft: Case of study. *Mechatronics*, 20(1), 143–152.

Liu, H., Pan, Y., Cao, J., Wang, H., and Zhou, Y. (2020). Adaptive neural network backstepping control of fractional-order nonlinear systems with actuator faults. *IEEE Transactions on Neural Networks and Learning Systems*, 31(12), 5166–5177.

Liu, H., Pan, Y., Li, S., and Chen, Y. (2017). Adaptive fuzzy backstepping control of fractional-order nonlinear systems. *IEEE Transactions on Systems, Man, and Cybernetics: Systems*, 47(8), 2209–2217.

Liu, T.K. and Juang, J.G. (2009). A single neuron pid control for twin rotor mimo system. In *2009 IEEE/ASME International Conference on Advanced Intelligent Mechatronics*, 186–191. IEEE.

Loutfi, B., Samir, Z., Ali, D., and Zinelaabidine, G.M. (2019). Real time implementation of type-2 fuzzy backstepping sliding mode controller for twin rotor mimo system (trms). *Traitement du Signal*, 36(1), 1–11.

Marconi, L. and Naldi, R. (2008). Aggressive control of helicopters in presence of parametric and dynamical uncertainties. *Mechatronics*, 18(7), 381–389.

Mihaly, V., Şuşcă, M., Morar, D., Stănese, M., and Dobra, P. (2021). μ-synthesis for fractional-order robust controllers. *Mathematics*, 9(8), 911.

Morari, M. and Zafiriou, E. (1989). *Robust process control*. Morari.

Ng, W.Y. (1988). *Interactive multi-objective programming as a framework for computer-aided control system design*. Ph.D. thesis, University of Cambridge.

Pratap, B. and Purwar, S. (2010). Neural network observer for twin rotor mimo system: an lmi based approach. In *Proceedings of the 2010 International Conference on Modelling, Identification and Control*, 539–544. IEEE.

Raghavan, R. and Thomas, S. (2017). Practically implementable model predictive controller for a twin rotor multi-input multi-output system. *Journal of Control, Automation and Electrical Systems*, 28(3), 358–370.

Rahideh, A., Bajodah, A.H., and Shaheed, M.H. (2012). Real time adaptive nonlinear model inversion control of a twin rotor mimo system using neural networks. *Engineering Applications of Artificial Intelligence*, 25(6), 1289–1297.

Saroj, D.K., Kar, I., and Pandey, V.K. (2013). Sliding mode controller design for twin rotor mimo system with a nonlinear state observer. In *2013 International Mutli-Conference on Automation, Computing, Communication, Control and Compressed Sensing (iMac4s)*, 668–673. IEEE.

Slavov, T., Mollov, L., Kralev, J., and Petkov, P. (2013). Real-time robust control using digital signal processor. *Balkan Journal of Electrical and Computer Engineering*, 1(2), 56–63.

Tastemirov, A., Lecchini-Visintin, A., and Morales, R.M. (2013). Complete dynamic model on the twin rotor mimo system (trms) with experimental validation.

Wen, P. and Li, Y. (2011). Twin rotor system modeling, de-coupling and optimal control. In *2011 IEEE International Conference on Mechatronics and Automation*, 1839–1842. IEEE.

Whidborne, J.F., Postlethwaite, I., and Gu, D.W. (1994). Robust controller design using h/sub/spl infin//loop-shaping and the method of inequalities. *IEEE Transactions on Control Systems Technology*, 2(4), 455–461.

Young, K.D., Utkin, V.I., and Ozguner, U. (1999). A control engineer's guide to sliding mode control. *IEEE transactions on control systems technology*, 7(3), 328–342.

Yu, G.R. and Liu, H.T. (2005). Sliding mode control of a two-degree-of-freedom helicopter via linear quadratic regulator. In *2005 IEEE International Conference on Systems, Man and Cybernetics*, volume 4, 3299–3304. IEEE.

Zakian, V. and Al-Naib, U. (1973). Design of dynamical and control systems by the method of inequalities. In *Proceedings of the Institution of Electrical Engineers*, volume 120, 1421–1427. IET.